Time-resolved determination of ortho-positronium kinetic energy utilizing *p*-wave scattering during positronium-xenon collisions

Kengo Shibuya,* Yoshihiro Kawamura, and Haruo Saito
Institute of Physics, Graduate School of Arts and Sciences, The University of Tokyo, Komaba 3-8-1, Meguro, Tokyo 153-8902, Japan
(Received 5 June 2013; published 29 October 2013)

We report a method to determine time evolution of ortho-positronium (*o*-Ps) kinetic energy with higher accuracy and sensitivity than conventional methods. Our method utilizes the fact that, during Ps-Xe collisions, an *o*-Ps atom can undergo a spin-conversion reaction induced by spin-orbit interaction to decay into two gamma-ray photons and the fact that the reaction rate strongly depends on the *o*-Ps kinetic energy because the reaction occurs only in *p*-wave scattering; thus a small change in the energy leads to a large change in the two-photon annihilation rate. Utilizing this reaction as a "lens" to magnify the *o*-Ps kinetic energy, we obtain its time evolution by measuring the time-resolved two-photon annihilation rate with an age-momentum correlation spectrometer. The time evolution of *o*-Ps kinetic energy can be explained by a classical model that assumes elastic collisions in a time range greater than 20 ns and an energy range of 40–60 meV. By applying this method, the Ps-Xe momentum-transfer cross section is found to be $12(2) \times 10^{-16}$ cm^2.

DOI: 10.1103/PhysRevA.88.042517 PACS number(s): 36.10.Dr, 34.80.Uv, 78.70.Bj

I. INTRODUCTION

Positronium (Ps) is the lightest hydrogenlike atom and formed in many gases and aggregates of ultrafine grains when an electron in atomic or molecular orbital is captured by a positron. A Ps atom decays into a few gamma-ray photons; three photons (each of energy less than 511 keV) are produced from a spin-triplet Ps (ortho-positronium, *o*-Ps) whose lifetime is $\tau_o = 142.04(1)$ ns in vacuum [1–5], whereas two photons (each of energy 511 keV) are produced from a spin-singlet Ps (para-positronium, *p*-Ps) whose lifetime is $\tau_p = 125.14(3)$ ps in vacuum [5–7]. The lifetime of an *o*-Ps is sufficiently long for it to experience many collisions with gas molecules and grain surfaces before its radiative decay. The initial *o*-Ps kinetic energy is a few electron volts. It quickly decreases via inelastic collisions above the first excitation energy of a target and very slowly decreases via elastic collisions below the first excitation energy since the mass of a Ps atom is much smaller than that of the target. It takes 10–100 ns for *o*-Ps to reach thermal equilibrium, and this long thermalization time causes considerable systematic uncertainty in precise determination of Ps properties, such as lifetime [1,8–11] and hyperfine structure [12–15]. This phenomenon prevents the precise tests of quantum electrodynamics.

Considerable efforts have been expended to determine the time evolution of Ps kinetic energy [$E(t)$]. As a result of these efforts, two methods have been developed; however their Ps kinetic energy resolution, time resolution, and sensitivity are insufficient to discuss the difference between experimental results and theoretical calculations [16–22]. The first method is the angular correlation of positron annihilation radiation (ACAR) technique, which measures the coincidence of two photons whose angular correlation deviation from 180° is proportional to $\sqrt{E(t)}$ in gases [16–18]. By using this technique, Nagashima *et al*. have obtained $\bar{E}(\tau)$, which is an averaged time evolution of Ps kinetic energy over the mean *o*-Ps lifetime (τ) changed by applying a magnetic field. However, it is difficult to obtain $E(t)$ by deconvoluting $\bar{E}(\tau)$. The second method is the Doppler-broadened spectra (DBS) technique, which measures the energy of a photon whose energy deviation from 511 keV is proportional to $\sqrt{E(t)}$ [19–22]. The Ps kinetic energy resolution of DBS is approximately ten times worse than that of ACAR. The typical gamma-ray energy resolution of a high-purity-germanium (HP-Ge) detector is 1 keV at 511 keV, which corresponds to a Ps kinetic energy resolution of 4 eV; this is two orders of magnitude larger than the thermal energy at room temperature. As a result, analyzing DBS data requires complex deconvolution of the system function as well as separation of overlapping spectral components by which the systematic and statistical uncertainties are increased. Furthermore, the low sensitivity of both techniques is partly because they detect two-photon annihilation of *o*-Ps induced by a magnetic field under which the spin state of *o*-Ps is mixed with that of *p*-Ps due to the Zeeman effect. Specifically, at 0.2 T, only one of six *o*-Ps atoms undergoes the two-photon annihilation to provide information on $E(t)$ [16–22]. These problems are resolved in our method.

One of the most important parameters when considering $E(t)$ in gases (i.e., Ps thermalization) is the momentum-transfer cross sections (σ_m). However, it is very difficult to predict σ_m because both the Ps and the gas molecule have internal structures [20–25]. Rather simple Ps-He collisions simulated by several models provide values for σ_m that differ by several times. To improve theoretical calculations, accurate experimental results are essential.

In this study, we demonstrate a method for measuring $E(t)$ with high accuracy and sensitivity to overcome the conventional problems. Our method is based on the fact that the *o*-Ps two-photon annihilation rate at time t [$\lambda_2(t)$] due to spin conversion induced by the spin-orbit interaction strongly depends on $E(t)$ [26–28]. This phenomenon results from the spin conversion occurring only in *p*-wave scattering of *o*-Ps with high-Z atoms in gas molecules. This reaction was theoretically proposed in 2003 [26], and was experimentally confirmed in 2006 [27]. Once *o*-Ps converts into *p*-Ps, annihilation of *p*-Ps

*shibuken@gakushikai.jp

into two gamma-ray photons is rapid because the annihilation rate of p-Ps ($\lambda_p = \tau_p^{-1} = 7.99 \times 10^9\ \mathrm{s}^{-1}$) is much greater than that of o-Ps ($\lambda_o = \tau_o^{-1} = 7.04 \times 10^6\ \mathrm{s}^{-1}$).

At the first step of analysis of the proposed method, $\lambda_2(t)$ is determined, and at the second step, $\lambda_2(t)$ is converted into $E(t)$. The analysis requires neither deconvolution of the system function nor separation of overlapping components. Moreover, no magnetic field is required and all o-Ps atoms are used to measure $E(t)$. As a result, the proposed method yields an $E(t)$ sufficiently accurate to allow meaningful comparison of theoretical calculations with the experimental results. Furthermore, as an application of this method, we determine σ_m in Ps-Xe collisions. This method can provide precious information not only for studies of Ps but also for studies of general atomic or molecular scattering because of the unique properties of Ps: A significant amount of information on the physics of atomic and molecular scattering is obtained by careful analysis of the annihilation radiation.

II. EXPERIMENT

The experimental setup is shown in Fig. 1. The positron source was 450 kBq (12 μCi) of ^{22}NaCl deposited on Ti foils. The source was sandwiched between 0.1 g cm^{-3} silica aerogel (SAG) used as a positron-positronium converter [16,29,30]. The source and SAG were positioned at the center of a stainless-steel chamber equipped with a turbomolecular pump, a pressure gauge, and a bottle of research-grade Xe gas. The gas pressure was maintained at 250.0 ± 0.5 kPa.

Six radiation detectors of two types were used: one HP-Ge detector (GC1518, Canberra), for a stop signal, and five BaF_2 scintillation detectors, one for stop and four for start signals. The start signal was due to a 1.27 MeV nuclear gamma ray, which was immediately emitted after positron emission and used to define $t = 0$, and the stop signal was due to annihilation radiation with energy below 511 keV, which was emitted during two- and three-photon annihilation. (i) The HP-Ge detector measured the energy of the stop signal. Its output via a preamplifier and a spectroscopy amplifier was transferred to a 14-bit digitizer (PXI-5122, National Instruments) at a 100 MHz sampling. The timing output of the preamplifier was transferred to NIM circuits. (ii) A scintillation detector located on the opposite sides of the chamber from the HP-Ge measured the timing of the stop signal. Its output was transferred to an 8-bit digital oscilloscope (WavePro7000, LeCroy) at a 1 GHz sampling and to the NIM circuits. (iii) The four other scintillation detectors measured the timing of the start signal. The four outputs were mixed and transferred to the oscilloscope and the NIM circuits.

Detecting triple coincidence among the start signal and the two stop signals, the NIM circuits sent a trigger signal to the oscilloscope and digitizer to make them transfer digitized wave forms to a PC. At the PC, the energy of the stop signal was obtained by a pulse height analysis and the time interval between the start and stop signals was obtained by a constant fraction method [31–33]. These events were accumulated in a two-dimensional array describing the relationship between the energy and the time interval, namely, age-momentum correlation (AMOC) data.

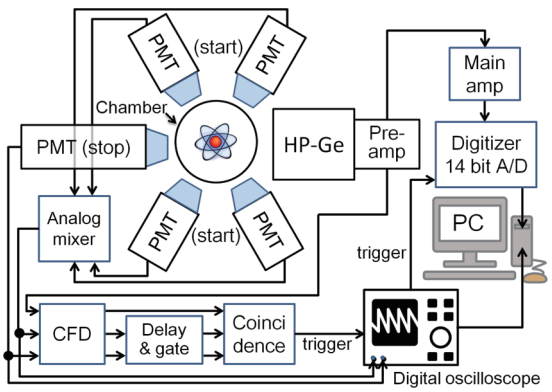

FIG. 1. (Color online) Schematic of the experimental setup. The NIM circuits consist of constant fraction discriminators (model 935, EG&G ORTEC), delay and gate stretchers (KN1500, Kaizu, Japan), and a coincidence unit (RPN130, REPIC, Japan).

III. RESULTS AND DICUSSION

A. Lifetimes spectra and two-photon-annihilation rate

The energy spectrum is shown in the insets of Figs. 2 and 3. By using the energy information, we create two kinds of lifetime spectra: a two-photon-annihilation lifetime spectrum [$I_2^{\mathrm{raw}}(t)$] and a three-photon-annihilation lifetime spectrum [$I_3^{\mathrm{raw}}(t)$]. $I_2^{\mathrm{raw}}(t)$ contains events in the full-energy peak (509–515 keV), where two-photon annihilation is mainly detected, whereas $I_3^{\mathrm{raw}}(t)$ contains events at the valley between the full-energy peak and the Compton edge (410–473 keV) where three-photon annihilation is mainly detected.

$I_2^{\mathrm{raw}}(t)$ and $I_3^{\mathrm{raw}}(t)$ possess background noise because of random coincidences, b_2 and b_3, respectively, whose values are determined by least-square fits using the fixed lifetime of $\tau_{\mathrm{fix}} = 101.4(6)$ ns determined previously [34]. We denote $I_2^{\mathrm{raw}}(t)$ after b_2 subtraction as $I_2(t)$, which is shown in Fig. 2. Contamination of the three-photon events in $I_2^{\mathrm{raw}}(t)$ is estimated to be less than 1% of the total counts of $I_2^{\mathrm{raw}}(t)$ and is ignored in our analysis. However, contamination of the two-photon events

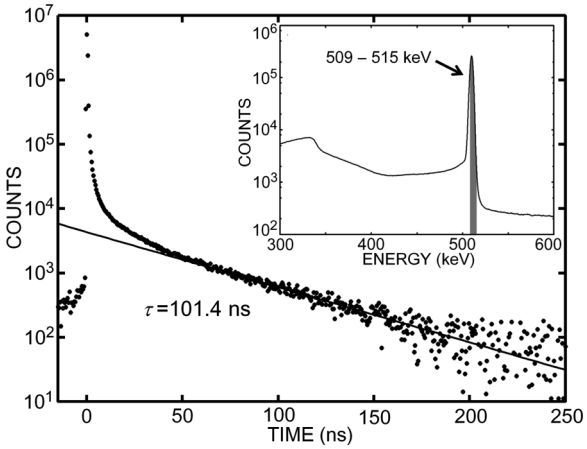

FIG. 2. Two-photon lifetime spectrum after background subtraction. The slope of the solid line corresponds to a lifetime of 101.4 ns. The inset shows the energy spectrum indicating the energy range of 509–515 keV.

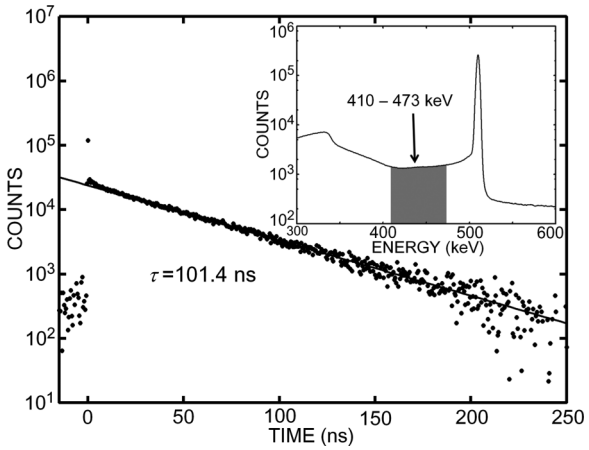

FIG. 3. Three-photon lifetime spectrum obtained by subtracting the random background and the contamination from two-photon events by setting $c = 0.0636$. The slope of the solid line corresponds to a lifetime of 101.4 ns. The inset shows the energy spectrum indicating the energy range of 410–473 keV.

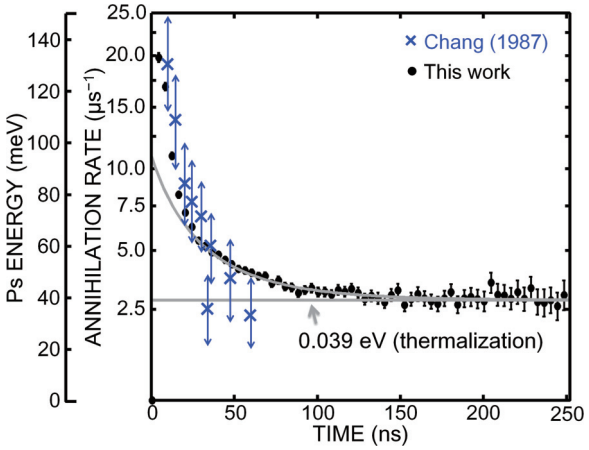

FIG. 4. (Color online) Time evolutions of o-Ps two-photon annihilation rate (inner y axis) and o-Ps energy (outer y axis). The y-axis units can be converted by using Eqs. (2) and (3a)–(3d). The fit is given by Eq. (4). The horizontal line at 0.039 meV indicates the thermal energy. For comparison, the Ps energy time evolution in silica aerogel measured by the Doppler-broadened spectrum technique of Chang [19] is shown by blue crosses.

in $I_3^{\rm raw}(t)$ is considerable. We estimate pure $I_3(t)$ as $I_3(t) \approx I_3^{\rm raw}(t) - cI_2^{\rm raw}(t) - b_3$, where c is a constant whose value is determined by requiring the peak at $t = 0$ to be adequately attenuated as shown in Fig. 3.

$I_2(t)$ and $I_3(t)$ are formulated as follows:

$$I_2(t) = I_2^{\rm raw}(t) - b_2 = \varepsilon_2 N(t)\lambda_2(t), \tag{1a}$$

$$I_3(t) = I_3^{\rm raw}(t) - cI_2^{\rm raw}(t) - b_3 = \varepsilon_3 N(t)\lambda_o, \tag{1b}$$

$$N(t) = N(0)\exp\left\{-\int_0^t [\lambda_2(t) + \lambda_o]\,dt\right\}, \tag{1c}$$

where ε_2 and ε_3 are detection efficiencies of the two-photon and three-photon annihilation, respectively, and $N(t)$ is the number of o-Ps atoms.

First, we obtain $\lambda_2(t)$ by dividing Eq. (1a) by Eq. (1b):

$$\lambda_2(t) = [\varepsilon_3/\varepsilon_2][I_2(t)/I_3(t)]\,\lambda_o. \tag{2}$$

Although ε_2 and ε_3 are unknown constants, the ratio $\varepsilon_3/\varepsilon_2$ can be determined by requiring that Eq. (2) be satisfied at any t. When thermal equilibrium is achieved, λ_2 and I_2/I_3 become constants as $\lambda_2(t)|_{t>160\ \rm ns} = \tau_{\rm fix}^{-1} - \lambda_o = 2.82(6) \times 10^6\ \ {\rm s}^{-1}$ and $[I_2(t)/I_3(t)|_{\,t>160\ \rm ns}]\lambda_o = 1.22(2) \times 10^7\ {\rm s}^{-1}$. Substitution of these values into Eq. (2) yields $\varepsilon_3/\varepsilon_2 = 0.231(6)$. Thus, we absolutely determine $\lambda_2(t)$ as shown in Fig. 4 (on the inner y axis).

B. Time evolution of *o*-Ps kinetic energy

Next, we convert $\lambda_2(t)$ into $E(t)$. From our previous study [34], λ_2 is known as a function of temperature (T):

$$\lambda_2(T) = \lambda_{\rm SC}^{\rm Xe}(T) + \lambda_{\rm PO}^{\rm Xe}(T) + \lambda_{\rm PO}^{\rm SAG}(T), \tag{3a}$$

$$\lambda_{\rm SC}^{\rm Xe}(T) = 8.27(19) \times T^{2.08(1)}, \tag{3b}$$

$$\lambda_{\rm PO}^{\rm Xe}(T) = 2.99(16) \times 10^3 \times T^{1.03(1)}, \tag{3c}$$

$$\lambda_{\rm PO}^{\rm SAG}(T) = 9.91(7) \times 10^4 \times T^{0.317(1)}, \tag{3d}$$

where $\lambda_{\rm SC}^{\rm Xe}$ is the o-Ps spin-conversion annihilation rate because of the spin-orbit interaction during Ps-Xe collision, $\lambda_{\rm PO}^{\rm Xe}$ is the o-Ps pick-off annihilation rate during Ps-Xe collision, and $\lambda_{\rm PO}^{\rm SAG}$ is the o-Ps pick-off annihilation rate for the SAG. Using Eqs. (2) and (3a)–(3d), we obtain the time evolution of o-Ps temperature [$T(t)$]. Finally, we use $E(t) = 3k_B T(t)/2$ to determine $E(t)$ as shown in Fig. 4 (on the outer y axis).

The curve fit in Fig. 4 is a hyperbola based on a classical model assuming elastic collisions and is formulated as follows [16,35]:

$$E(t) = E_{\rm th}\coth^2(\alpha + \beta t), \tag{4}$$

where $E_{\rm th} = E|_{t=\infty}$ is thermal energy, $\alpha = \coth^{-1}\sqrt{E|_{t=0}/E_{\rm th}}$, and $\beta = p_{\rm th}(\sigma_{\rm m} n/M_{\rm Xe} + 1/LM_{\rm SAG})$ with thermalized Ps momentum ($p_{\rm th}$), density number of Xe atoms (n), mass of a Xe atom ($M_{\rm Xe}$), mean distance between silica ultrafine grains (L), and effective mass of SAG in the collision ($M_{\rm SAG}$). The first term of β, i.e., $\beta_{\rm Xe} = p_{\rm th}\,\sigma_{\rm m} n/M_{\rm Xe}$ is a thermalization factor due to Ps-Xe elastic collisions. The second term, $\beta_{\rm SAG} = p_{\rm th}/LM_{\rm SAG}$, is a thermalization factor due to Ps-SAG elastic collisions.

From the measurement at 250 kPa, we obtain $\alpha = 9.4(2) \times 10^{-2}$ and $\beta^{-1} = 89(2)$ ns by a least-squares fitting. Equation (4) well reproduces the o-Ps kinetic energy in a time range later than 20 ns. Prior to this time, the model does not match the results. One reason for this discrepancy is two-photon annihilation of p-Ps atoms and free positrons, which are not included in the model. Another reason is that σ_m is considered to be constant, although it can change as a function of the o-Ps kinetic energy. In other words, the goodness of the fit after 20 ns means that σ_m is constant within the uncertainty for the energy range 40–60 meV.

At low temperatures, Hg atoms (ground state: ^1S) adsorbed onto SAG can be used instead of Xe gas molecules to increase the sensitivity of this method by several times because the spin-conversion cross section is approximately proportional to Z^5 [26]. A possible application may be a thermometer for Bose-Einstein condensates of Ps in SAG [36–41].

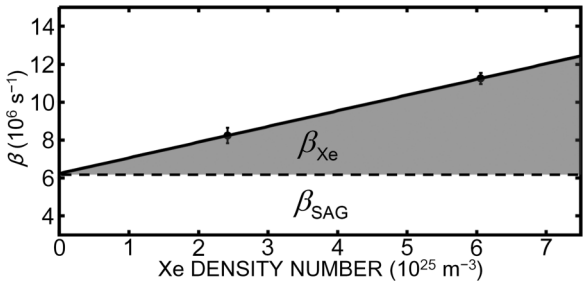

FIG. 5. Thermalization factor due to Ps-Xe elastic collisions (β_{Xe}) and that due to Ps-SAG elastic collisions (β_{SAG}) as a function of Xe number density. The two measurement points are at 100 and 250 kPa. The horizontal dashed line indicates $\beta_{SAG} = 6.2(7) \times 10^6\ s^{-1}$. From the slope of the fit, we determined $\sigma_m = 12(2) \times 10^{-16}\ cm^2$.

C. Momentum-transfer cross section during Ps-Xe collisions

As an application, we determined σ_m in Ps-Xe collisions. A similar AMOC measurement was performed at 100 kPa gaseous Xe to obtain $\alpha = 9.9(5) \times 10^{-2}$ and $\beta^{-1} = 121(6)$ ns. Then, as shown in Fig. 5, we determined $\beta_{Xe} = 5.0(8) \times 10^6\ s^{-1}$ at 250 kPa, $\beta_{Xe} = 2.0(3) \times 10^6\ s^{-1}$ at 100 kPa, and $\beta_{SAG} = 6.2(7) \times 10^6\ s^{-1}$. Finally, from the slope of the fit, we determined $\sigma_m = 12(2) \times 10^{-16}\ cm^2$ in the energy range of 40–60 meV. σ_m in other energy ranges can be obtained by measurements at lower and higher temperatures, which is left for future study.

The σ_m in Ps-Xe collisions has not been reported previously, however, we find it is comparable with $\pi r_w^2 = 14.7 \times 10^{-16}\ cm^2$, where $r_w = 2.16 \times 10^{-10}$ m is the van der Waals radius of Xe. For electron-xenon collisions at around 40 meV, larger values for σ_m have been reported both experimentally ($23 \times 10^{-16}\ cm^2$ [42], $40 \times 10^{-16}\ cm^2$ [43], $60 \times 10^{-16}\ cm^2$ [44]) and theoretically ($48 \times 10^{-16}\ cm^2$ [45], $60 \times 10^{-16}\ cm^2$ [46]), which is natural because a Ps atom is neutral whereas an electron is charged.

We are going to measure the Ps momentum-transfer cross sections for various gas molecules by mixing them with Xe. β in Eq. (4) can be described as $\beta = \beta_{SAG} + \beta_{Xe} + \beta_{sample}$, where β_{sample} is a thermalization factor due to elastic collisions of Ps and the sample gas molecules.

IV. CONCLUSION

We determined the time evolution of the o-Ps kinetic energy by utilizing the fact that the o-Ps two-photon annihilation rate strongly depends on the o-Ps kinetic energy because the ortho-para spin conversion caused by the spin-orbit interaction during Ps-Xe collisions occurs only in p-wave scattering. We obtained the absolute value of the time evolution of the o-Ps kinetic energy from the o-Ps two-photon annihilation rate measured with an AMOC spectrometer. We investigated that the thermalization process is well explained by the classical model assuming elastic collisions below 60 meV, and determined that the momentum-transfer cross section during Ps-Xe collisions is $\sigma_m = 12(2) \times 10^{-16}\ cm^2$.

ACKNOWLEDGMENT

We gratefully acknowledge financial support from the Japan Society for the Promotion of Science (KAKENHI, 23654114).

[1] S. Asai, S. Orito, and N. Shinohara, Phys. Lett. B **357**, 475 (1995).
[2] R. S. Vallery, P. W. Zitzewitz, and D. W. Gidley, Phys. Rev. Lett. **90**, 203402 (2003).
[3] Y. Kataoka, S. Asai, and T. Kobayashi, Phys. Lett. B **671**, 219 (2009).
[4] G. S. Adkins, R. N. Fell, and J. Sapirstein, Phys. Rev. Lett. **84**, 5086 (2000).
[5] B. A. Kniehl and A. A. Penin, Phys. Rev. Lett. **85**, 1210 (2000).
[6] A. H. Al-Ramadhan and D. W. Gidley, Phys. Rev. Lett. **72**, 1632 (1994).
[7] A. Czarnecki, K. Melnikov, and A. Yelkhovsky, Phys. Rev. Lett. **83**, 1135 (1999).
[8] C. I. Westbrook, D. W. Gidley, R. S. Conti, and A. Rich, Phys. Rev. A **40**, 5489 (1989).
[9] J. S. Nico, D. W. Gidley, A. Rich, and P. W. Zitzewitz, Phys. Rev. Lett. **65**, 1344 (1990).
[10] G. S. Adkins, A. A. Salahuddin, and K. E. Schalm, Phys. Rev. A **45**, 7774 (1992).
[11] P. Labelle, G. P. Lepage, and U. Magnea, Phys. Rev. Lett. **72**, 2006 (1994).
[12] B. A. Kniehl and A. A. Penin, Phys. Rev. Lett. **85**, 5094 (2000).
[13] S. G. Karshenboim, Phys. Rep. **422**, 1 (2005).
[14] A. Ishida, Y. Sasaki, G. Akimoto, T. Suehara, T. Namba, S. Asai, T. Kobayashi, H. Saito, M. Yoshida, K. Tanaka, and A. Yamamoto, arXiv:1004.5555.
[15] A. Ishida, Y. Sasaki, G. Akimoto, T. Suehara, T. Namba, S. Asai, T. Kobayashi, H. Saito, M. Yoshida, K. Tanaka, and A. Yamamoto, Hyperfine Interact. **212**, 133 (2012).
[16] Y. Nagashima, M. Kakimoto, T. Hyodo, K. Fujiwara, A. Ichimura, T. Chang, J. Deng, T. Akahane, T. Chiba, K. Suzuki, B. T. A. McKee, and A. T. Stewart, Phys. Rev. A **52**, 258 (1995).
[17] Y. Nagashima, T. Hyodo, K. Fujiwara, and A. Ichimura, J. Phys. B **31**, 329 (1998).
[18] F. Saito, Y. Nagashima, and T. Hyodo, J. Phys. B **36**, 4191 (2003).
[19] T. Chang, M. Xu, and X. Zeng, Phys. Lett. A **126**, 189 (1987).
[20] M. Skalsey, J. J. Engbrecht, R. K. Bithell, R. S. Vallery, and D. W. Gidley, Phys. Rev. Lett. **80**, 3727 (1998).
[21] M. Skalsey, J. J. Engbrecht, C. M. Nakamura, R. S. Vallery, and D. W. Gidley, Phys. Rev. A **67**, 022504 (2003).
[22] J. J. Engbrecht, M. J. Erickson, C. P. Johnson, A. J. Kolan, A. E. Legard, S. P. Lund, M. J. Nyflot, and J. D. Paulsen, Phys. Rev. A **77**, 012711 (2008).
[23] I. A. Ivanov, J. Mitroy, and K. Varga, Phys. Rev. A **65**, 032703 (2002).

[24] A. Basu, P. K. Sinha, and A. S. Ghosh, Phys. Rev. A **63**, 052503 (2001).
[25] S. Chiesa, M. Mella, and G. Morosi, Phys. Rev. A **66**, 042502 (2002).
[26] J. Mitroy and S. A. Novikov, Phys. Rev. Lett. **90**, 183202 (2003).
[27] H. Saito and T. Hyodo, Phys. Rev. Lett. **97**, 253402 (2006).
[28] H. Saito, T. Nakayama, and T. Hyodo, J. Phys. Conf. Ser. **194**, 012038 (2009).
[29] G. Poelz and R. Riethmuller, Nucl. Instrum. Methods **195**, 491 (1982).
[30] D. B. Cassidy, P. Crivelli, T. H. Hisakado, L. Liszkay, V. E. Meligne, P. Perez, H. W. K. Tom, and A. P. Mills, Jr., Phys. Rev. A **81**, 012715 (2010).
[31] H. Saito, Y. Nagashima, T. Kurihara, and T. Hyodo, Nucl. Instrum. Methods A **487**, 612 (2002).
[32] H. Saito and T. Hyodo, Radiat. Phys. Chem. **68**, 431 (2003).
[33] H. Saito and T. Hyodo, Phys. Rev. Lett. **90**, 193401 (2003).
[34] K. Shibuya, T. Nakayama, H. Saito, and T. Hyodo, Phys. Rev. A **88**, 012511 (2013).
[35] W. C. Sauder, J. Res. Natl. Bur. Stand. Sect. A **72A**, 91 (1968).
[36] P. M. Platzman and A. P. Mills, Jr., Phys. Rev. B **49**, 454 (1994).
[37] K. Oda, T. Miyakawa, H. Yabu, and T. Suzuki, J. Phys. Soc. Jpn. **70**, 1549 (2001).
[38] H. Saito and T. Hyodo, in *New Directions in Antimatter Chemistry and Physics*, edited by C. M. Surko and F. A. Gianturco (Kluwer, Dordrecht, 2001), p. 101.
[39] D. B. Cassidy and J. A. Golovchenko, in *New Directions in Antimatter Chemistry and Physics*, edited by C. M. Surko and F. A. Gianturco (Kluwer, Dordrecht, 2001), p. 83.
[40] D. B. Cassidy, S. H. M. Deng, R. G. Greaves, T. Maruo, N. Nishiyama, J. B. Snyder, H. K. M. Tanaka, and A. P. Mills, Jr., Phys. Rev. Lett. **95**, 195006 (2005).
[41] D. B. Cassidy and A. P. Mills, Jr., Phys. Status Solidi C **4**, 3419 (2007).
[42] C. L. Chen, Phys. Rev. **131**, 2550 (1963).
[43] C. R. Hoffmann and H. M. Skarsgard, Phys. Rev. **178**, 168 (1969).
[44] M. Suzuki, T. Taniguchi, N. Yoshimura, and H. Tagashira, J. Phys. D **25**, 50 (1992).
[45] T. Koizumi, E. Shirakawa, and I. Ogawa, J. Phys. B **19**, 2331 (1986).
[46] L. S. Frost and A. V. Phelps, Phys. Rev. **136**, A1538 (1964).